Published in final edited form as:
Phys Med Biol. 2004 September 21; 49(18): 4207–4218.

Viscoelastic characterization of *in vitro* canine tissue

Miklos Z Kiss[1], **Tomy Varghese**[1,2], and **Timothy J Hall**[1]

1 *Department of Medical Physics, 1300 University Avenue, Room 1530, University of Wisconsin, Madison, WI 53706, USA*

2 *Department of Biomedical Engineering, 1550 Engineering Drive, Room 2130, University of Wisconsin, Madison, WI 53706, USA*

Abstract

Mechanical properties of biological tissues are of interest for assessing the performance of elastographic methods that evaluate the stiffness characteristics of tissue. The mechanical properties of interest include the frequency-dependent complex moduli, storage and loss moduli of tissues. Determination of the mechanical properties of biological tissues is often limited by proper geometry of the sample, as well as homogeneity of the stress–strain relationship. Measurements were performed on *in vitro* canine liver tissue specimens, over a frequency range from 0.1 to 400 Hz. Tests were conducted using an EnduraTEC ELF 3200, a dynamic testing system for determining the mechanical properties of materials. Both normal tissues and thermal lesions prepared by radio frequency ablation were tested. Experiments were conducted by uniaxially compressing tissue samples using Plexiglas platens larger than the specimens and measuring the load response. The resulting moduli spectra were then fit to a modified Kelvin–Voigt model, called the Kelvin–Voigt fractional derivative model. The data agree well with the model and in comparing the results from the normal tissue with that of the thermal lesions, the concept of a complex modulus contrast is introduced and its applications to elastography are discussed.

1. Introduction

Testing and modelling of the mechanical properties of biological soft tissues presents a unique set of challenges, since many of them are nonlinear, viscoelastic and anisotropic (Fung 1993). Since benign and malignant processes can both alter the mechanical tissue properties, elastography, a new imaging modality, was developed to exploit this by relying on the tissues' elastic modulus as the major contrast mechanism (Dickinson and Hill 1982, Wilson and Robinson 1982, Ophir *et al* 1991). However, the reliability of elastography partly depends on the accuracy of the values used for the elastic modulus. Despite this need for determining the available modulus contrast, there is very little reliable data available on soft tissue properties. Several groups have published findings on the mechanical properties of soft tissues, and the methods vary as widely as the values reported (Suki *et al* 1994, Arbogast and Margulies 1998, Erkamp *et al* 1998, Kim *et al* 1999, Lakes and Vanderby 1999, Yuan *et al* 2000, Darvish and Crandall 2001, Schwartz *et al* 2001, Nasseri and Bilston 2002, Lippert and Grimm 2003). In addition, the concentration in these reports was lung, tendon, brain or kidney. There are fewer reports published concerning tissues such as liver, breast or prostate, or even tissue mimicking materials (Chen *et al* 1996, Hall *et al* 1997, Krouskop *et al* 1998, Liu and Bilston 2000, Yeh *et al* 2002, Moffit *et al* 2002, Han *et al* 2003, Sammani *et al* 2003, Ishihara *et al* 2003).

Of the articles in the literature covering the viscoelastic properties for liver, breast and prostate, two are of particular interest because the experimental methods used include dynamic testing (Krouskop *et al* 1998, Liu and Bilston 2000). When a viscoelastic solid is subjected to oscillatory strains, the modulus (both axial and shear) is a complex quantity, with both real

(elastic) and imaginary (viscous) components. Krouskop *et al* investigated the viscoelastic properties of breast and prostate tissues (normal, benign and malignant) at low frequencies (0.1, 1.0, 4.0 Hz) (Krouskop *et al* 1998). The group reported elastic modulus values 18–500 kPa in breast tissue for various amounts of precompression loading. Normal tissues had significantly lower values than the cancerous tissues. Although values for the complex modulus were not reported, they did note that the phase shift was less than 10°. The tangent of the phase angle is the ratio of the imaginary component of the complex modulus to the real component. Such a small phase angle indicates a very small viscous response in the tissues at the frequencies reported.

Liu and Bilston investigated bovine livers and reported results for the complex shear modulus in the range of 0.006–20 Hz, with the real component in the range of 1–6 kPa (increasing proportionately to frequency), and the imaginary component in the range of several hundred Pa for the same frequencies (Liu and Bilston 2000). They fit the frequency-dependent moduli to a generalized five-element Maxwell model (Fung 1993).

The choice of model for fitting data seems to vary with the reports. In addition to Liu and Bilston's work, Nasseri *et al* measured the frequency-dependent modulus of porcine kidneys and fit the data to a power law (Nasseri and Bilston 2002). Several other authors have investigated the use of power law models (Bagley and Torvik 1983, Suki *et al* 1994, Szabo and Wu 2000, Chen *et al* 2003). The three models described by Fung (1993) are essentially linear, and these four references include justifications for using quasi-linear or nonlinear models to relate the stress to the strain in biological tissue. In particular, they introduce a fractional derivative model, and one of them (Suki *et al* 1994) carefully compares the pros and cons of competing models (nonlinear constitutive equation, differential equations with time-dependent coefficients, continuous distribution of time constants that are solutions to integral equations and complex dynamic systems exhibiting self-similar properties).

In this study, canine liver samples were subjected to dynamic loading in the range of 0.1–400 Hz and the resulting force response was measured. The complex modulus was calculated and fit to a Kelvin–Voigt fractional derivative (KVFD) model, which combines the well-known Kelvin–Voigt (or Voigt) (KV) model with the fractional derivative approach as described by others (Bagley and Torvik 1983, Suki *et al* 1994, Chen *et al* 2003, Taylor *et al* 2001, 2002, 2003). Both normal tissue and thermal lesions, prepared by radio frequency (rf) ablation, were tested and the results are shown in the following sections. The results of one group have been recently presented at conferences describing the results of dynamic loading experiments conducted on bovine liver (Moskowitz *et al* 2001, Taylor *et al* 2001, 2002, 2003). While the results presented agree well with the KVFD model, the low number of specimens studied limits the statistical significance of the findings. This paper presents findings with a higher level of statistical significance and fills a gap in the literature concerning the use of the KVFD model applied to tissue.

2. Theory

The viscoelastic behaviour of biological tissue can be measured experimentally using a variety of methods. One of these methods relies on applying a compressive displacement $x(t)$ to a slab of material of uniform thickness, $d(t)$, and cross-sectional area $A(t)$, and measuring the force response $F(t)$. If the displacement is cyclic, that is, $x(t) \sim e^{i\omega t}$, then the cyclic strain ε is the displacement divided by the sample thickness. The resultant stress σ is then the force response divided by the cross-sectional area, in other words, $\sigma = F(t)/A(t)$. For a homogeneous, purely elastic medium, the basic constitutive equation relating the stress to the strain, ε, is

$$\sigma = E\varepsilon, \tag{1}$$

where E is the Young's modulus of the sample. Most tissues, however, are viscoelastic, and therefore require additional terms to describe this behaviour. In a viscoelastic material, the stress response depends not only on the strain but also on the strain rate, or something akin to it, as will be illustrated below. Several viscoelastic models exist which incorporate this idea (Fung 1993). The KV model is of particular interest in this research. The stress is related to both the strain as well as the strain rate, $\dot{\varepsilon}(t)$, by

$$\sigma(t) = E\varepsilon(t) + \eta\,\dot{\varepsilon}\,(t), \tag{2}$$

where E is the material's elasticity and η is the viscosity parameter. When a viscoelastic material is subjected to cyclic strains, the stress response is necessarily cyclic, shifted by some phase angle, and the Young's modulus is replaced by a complex quantity, demonstrated in the following derivation. Fung and others derive the relations more rigorously, so the derivation is presented as a review. By taking the Fourier transform of both sides of equation (2), assuming the stress, strain and strain rate are cyclic (i.e., ε, $\sigma \sim e^{i\omega t}$, the KV model can be expressed in the frequency domain:

$$\sigma(w) = E\varepsilon(\omega) + i\omega\eta\varepsilon(\omega), \tag{3}$$

where, ω is the angular frequency in rad s^{-1}. Recalling the constitutive relation in equation (1), the modulus can be expressed as a complex quantity,

$$E^*(\omega) = E + i\omega\eta. \tag{4}$$

The real part of the complex modulus is known as the storage modulus, as it is an indicator of the material's ability to store energy. The imaginary part is known as the loss modulus, related to the amount of energy lost through viscous processes. In addition, the ratio of the imaginary to real part of the modulus is equal to the tangent of the phase angle δ, the angle by which the displacement leads the force response, and is called the loss tangent:

$$\tan\delta = \frac{\omega\eta}{E}. \tag{5}$$

This model is attractive due to its simplicity and relatively easy solution, but several researchers have noted that the model is insufficient in predicting the frequency-dependent complex modulus for viscoelastic media (Bagley and Torvik 1983, Szabo and Wu 2000, Suki *et al* 1994, Taylor *et al* 2001, 2002, 2003). The KV model accounts for both the storage and dissipation of energy (the elastic and viscous parameters, respectively), but it does not model relaxation. The model can be expanded to a standard linear solid by including multiple Kelvin–Voigt bodies in series, but the choice of an appropriate number of terms seems arbitrary (Suki *et al* 1994). Therefore, an improved model is required, and for this study, the fractional derivative representation of the KV model was chosen. It is almost as simple as the KV model, but the solutions have demonstrated better agreements with empirical results, with the major difference being that the second term in equation (2) is replaced with a fractional time derivative, such that

$$\sigma(t) = E\varepsilon(t) + \eta D^{\alpha}[\,\varepsilon(t)], \tag{6}$$

where the fractional derivative operator $D^{\alpha}[\ ]$ is defined by

$$D^{\alpha}[\,x(t)] = \frac{1}{\Gamma(1-\alpha)}\int_0^t \frac{x(\tau)}{(t-\tau)^{\alpha}}d\tau, \tag{7}$$

where Γ is the gamma function, and $x(t)$ is an integrable, harmonic function. Fractional derivatives behave similarly to power law functions when subjected to Fourier transforms. The Fourier transform of the fractional derivative is given by

$$\Im\{D^{\alpha}[x(t)]\} = (i\omega)^{\alpha}\Im[x(t)]. \tag{8}$$

Equation (8) is analogous to the Fourier transform of a derivative function. Taking the Fourier transform of equation (6) and including the results from equation (8) the KVFD model in frequency space is given by

$$\sigma(\omega) = E\varepsilon(\omega) + \eta(i\omega)^{\alpha}\varepsilon(\omega). \tag{9}$$

The frequency-dependent complex modulus in equation (9) is expressed as

$$E^{*}(\omega) = E + \eta(i\omega)^{\alpha}. \tag{10}$$

Equation (10) can be expanded using de Moivre's theorem ($e^{i\theta} = \cos\theta + i\sin\theta$), and recognizing that $i^{\alpha} = (e^{i\pi/2})^{\alpha} = \cos(\pi\alpha/2) + i\sin(\pi\alpha/2)$, the complex modulus can be expressed as

$$E^{*}(\omega) = \left[E + \eta\cos\left(\frac{\pi\alpha}{2}\right)\omega^{\alpha}\right] + i\left[\eta\sin\left(\frac{\pi\alpha}{2}\right)\omega^{\alpha}\right], \tag{11}$$

where the real and imaginary parts are shown within the brackets, and are denoted by E' and E'', respectively. The phase angle term is now given by

$$\tan\delta = \frac{\eta\omega^{\alpha}\sin\frac{\pi\alpha}{2}}{E + \eta\omega^{\alpha}\cos\frac{\pi\alpha}{2}}. \tag{12}$$

Equations (11) and (12) sufficiently characterize the complex modulus as a function of frequency for the specimens of interest, and it should be noted that they reduce to equations (4) and (5), respectively for $\alpha = 1$ (i.e., the KV model). Equation (11) is of particular interest, and it is this relationship that is investigated experimentally in the following sections.

3. Materials and methods

Canine livers were obtained from 8 to 9-month-old male hounds available from unrelated studies in an adjacent lab. Measurements were made within 72 h after death. Samples without lesions were cut from regions of tissue lacking any major vasculature or bile ducts using a custom-made cylindrical cutting tool 20 mm in diameter, and then sliced to an appropriate thickness (nominally 5 mm). These specimens were then placed in an isotonic saline bath at room temperature prior to testing. Tissue lesions were prepared using radio frequency (rf) ablation using a Rita Model 1500 (Rita Medical Systems, Inc., Mountain View, CA), prior to cutting to specimen size. Samples were subjected to three ablation protocols: 80 °C for 10 min, 90 °C for 10 min and 90 °C for 5 min.

After the samples had been placed in isotonic saline for at least 45 min to bring them to room temperature, they were placed in the dynamic testing system, an EnduraTEC ELF 3220 (EnduraTEC, Minnetonka, MN). The ELF 3220 is a tabletop testing system capable of dynamic testing frequencies from 10^{-5} to 400 Hz. The system is electromagnetic, and relies on rare-earth magnets placed in the field created by stationary windings to produce a linear force proportional to the field polarity and intensity. Acrylic platens were mounted to both the mover and the load cell. The platens were then coated with mineral oil to promote free-slip conditions between the specimen and the platens. The specimens were preloaded via compression to 2%

strain, and then compressed an additional 2%. The minimum and maximum strain values were determined by a ramp test to be within the linear regime of stress–strain response for all tissues. All measurements were performed at room temperature (21.0 ± 1.5 °C). The specimen was sequentially loaded at frequencies from 0.1 Hz up to 400 Hz. For each testing frequency, the specimen was held at a mean strain level (3%) for 5 s, after which the mover oscillated at the testing frequency. The system oscillated for 3 s prior to data acquisition to allow for transient decay and for the system to achieve the proper amplitude. Values for the complex modulus were obtained using the dynamic mechanical analysis (DMA) software for the ELF system.

Samples from ten animals were used for both the normal tissue and the lesion prepared at 90 °C and 10 min, and samples from five animals were used for the other two thermal lesion protocols.

4. Results

The following section presents the results of the previously described experiments. A useful way of expressing equation (11) is by taking the magnitude of $E^*(\omega)$:

$$\left|E^*(f)\right| = \sqrt{E_0^2 + 2E_0\eta(2\pi f)^\alpha \cos\frac{\pi\alpha}{2} + \eta^2(2\pi f)^{2\alpha}}, \tag{13}$$

where ω has been replaced with $2\pi f$. Figure 1 is a plot of $|E^*(f)|$ for the normal tissue and three lesion types. Each data point represents the average value taken over the total number of specimens tested for each condition (normal or lesion), and error bars represent one standard deviation from the mean. The rapid fluctuations in the normal tissue modulus at high frequencies are believed to be an electronic signal-to-noise ratio artefact in the force measurement. At these frequencies, it is likely that the load cell cannot distinguish between ambient system noise and the response due to the tissue. Note that this artefact exists only for the normal, unablated tissue. It is possible that measuring the shear modulus will lead to more reasonable results at high frequencies.

Figure 2(a) shows the real and imaginary parts of the complex modulus for normal tissue and the thermal lesion prepared at 90 °C for 10 min. The modulus estimates were also averaged over the number of trials. From this figure, it is clear that the real part of the complex modulus is greater than the imaginary part at low frequencies by as much as a factor of 5 for the normal tissue and a factor of 3 for the thermal lesion. The relationship between the real and imaginary parts of the complex modulus is represented in figure 2(b) in terms of the loss tangent as a function of frequency. Only data whose values are between 0 and 1 are presented, and the frequency range is limited to 100 Hz. The loss tangent is comparatively flat over three decades of frequency with a rapid rise at frequencies above 10 Hz.

The data in figure 1 were fit to equation (13) using the Levenberg–Marquardt method for nonlinear least squares fitting, and are plotted in figure 3, once again as a function of f. The high-frequency deviations from the best-fit curves for all cases is the result of generating a fit in the frequency range of 0.1–100 Hz, the region which the data most closely conformed to the model. Table 1 shows the best-fit parameters for each case, plus the χ^2 and R^2 values. The deviations may also indicate the presence of experimental artefacts, similar to that reported by Taylor (Taylor *et al* 2003). The data were also fit to the conventional KV model ($\alpha = 1$), and the parameters, χ^2 and R^2 values are shown in table 2.

Figure 4 is a plot of the real and imaginary parts of the complex modulus for the thermal lesion prepared at 90 °C for 10 min (figure 4(a)), and for the normal tissue (figure 4(b)) fitted to both the KVFD and KV models. The agreement between the data and the model is better for the

real part than it is for the imaginary part, and there is a clear improvement in the agreement between the data and the KVFD model compared to the KV model.

5. Discussion

The findings here accomplish two important things. First, this paper fills a gap in the literature with respect to using a fractional derivative model to study the viscoelastic properties of a biological system. The papers (Suki *et al* 1994, Chen *et al* 2003, Taylor *et al* 2001, 2002, 2003, Moskowitz *et al* 2001), form the bulk of the literature in this area. The strong empirical agreement between model and data suggests a need to investigate the application of such models to biological systems. The second accomplishment is that the fractional derivative model may allow for an expansion of the elastographic model to account for viscoelastic effects. This is seen clearly in a comparison of the data presented in tables 1 and 2. The χ^2 values for the KVFD model (table 1) are at least one order of magnitude smaller than their counterparts in for the KV model (table 2). Furthermore, the KVFD model predicts a comparatively lower value for E_0 than the KV model, and a comparatively higher value for η than the KV model. In the KV model, the E_0 is roughly two orders of magnitude larger than η for all tissues, while the difference in the KVFD model is less than one order of magnitude. Finally, the relative errors on the fit parameters are reduced with the KVFD model. The inclusion of a third parameter (namely, α) has a positive impact on the agreement of the model to the data. Graphically, the results in figure 4 clearly indicate a stronger agreement between data and model for the KVFD model than for the KV model. This is partly because the KV model does not have strong frequency dependence, which is present in the data. The real part of the complex modulus in the KV model is constant and the corresponding imaginary part varies linearly. It should be noted that in fitting the data to the KVFD model, the real part agrees better with the model than does the imaginary part. This is likely due to the fact that the parameters were determined using the magnitude of the complex modulus, which tends to be dominated by the real part, and therefore the contribution from the imaginary part is less significant than the contribution from the real part. Future investigations will include improving parameter estimation.

Besides the good agreement between model and data, comparison between the various lesion types reveals that the tissue properties seem to be more sensitive to maximum temperature rather than to ablation time. According to figures 1 and 3, the magnitude of the complex modulus for the lesion prepared at 90 °C for 10 min is approximately 1.5 times larger than that of the lesion prepared at 80 °C. The lesion prepared for only 5 min (at 90 °C) has a modulus that is only slightly lower than the 10 min counterpart. Also, in considering the results in figure 2, the lesion prepared at 90 °C for 10 min is not only stiffer than the normal tissue, as seen in figure 2(a), but inspection of the loss tangent as a function of frequency (figure 2(b) shows that it is also more viscoelastic over all frequencies, although the difference is relatively small (0.3 for the lesion and 0.2 for the normal tissue) at the lowest frequency. The rapid rise in loss tangent at frequencies above 10 Hz is attributed to the corresponding rapid rise in the loss modulus compared to the slow rise in storage modulus.

The major contributing factor to image contrast in elastography is the modulus contrast, i.e., the ratio of the elastic moduli of the inclusion to the background. An elastographic model that incorporates viscoelastic effects requires a new definition of the modulus contrast. The elastic modulus contrast is defined as

$$C_t \equiv \frac{E_I}{E_B}, \tag{14}$$

where E_I, and E_B are the elastic moduli of the inclusion and background, respectively (Kallel *et al* 1996). It should be noted that Kallel refers to the modulus contrast as the 'true target elasticity contrast'. Replacing the E_I and E_B with their complex counterparts gives a complex modulus contrast. Developing a viscoelastic model analogous to Kallel's is beyond the scope of this paper, but introducing a complex modulus contrast is an important first step. Recalling equation (11) and defining the real part as E' and the imaginary part as E'' the complex modulus contrast is defined as

$$C_t^* \equiv \frac{E_I' E_B' + E_I'' E_B''}{\left|E_B^*\right|^2} + \mathrm{i}\frac{E_I'' E_B' - E_I' E_B''}{\left|E_B^*\right|^2}, \tag{15}$$

where $\left|E_B^*\right|^2 = E_B'^2 + E_B''^2$.

Figure 5 shows a plot of the magnitude, as well as the real and imaginary parts of $C_t^*(f)$ with the assumption that the E_I' and E_I'' are determined by the best-fit parameters for the three lesions and E_B' and E_B'' are determined by the best-fit parameters for the normal tissue. In principle, it is possible for the imaginary part of equation (15) to be negative, but its impact on image contrast is not yet clear. What is clear from the graph is that the C_t^* for the lesion prepared at 90 °C for 10 min has the largest contrast. $\left|C_t^*\right|$ also possesses a local minimum near 0.3 Hz. The dip in the curve is due largely to the difference in the α values for the two tissues (as shown in table 1). The lesion's α-value is 2.7 times larger than the normal tissue's. For the other lesion at 90 °C, the ratio of the α-values is 2.1 and the minimum contrast is at 1 Hz. Finally, for the 80 °C lesion, the ratio is 2.3 and the minimum contrast is around 0.2 Hz. This may suggest that in determining the contribution of viscoelastic properties to image contrast, the elastogram may be best acquired at quasi-static to low frequency (less than 10 Hz) conditions. Although C_t^* generally increases with frequency, the merits of utilizing high frequency oscillating stimuli for elastography have not been considered here, and are beyond the scope of this paper. The high-frequency experimental artefacts present in normal tissue data currently limit the accuracy in this regime. It is expected that as the artefacts are removed, a model for high frequency elastography can be developed and improved.

6. Conclusion

The frequency-dependent complex modulus has been measured for *in vitro* canine liver, for both normal tissue and thermal lesions prepared by rf ablation. Results were fit to the conventional Kelvin–Voigt and Kelvin–Voigt fractional derivative models. There was excellent agreement between the data and the KVFD model, particularly at frequencies less than 100 Hz. The data deviated from the model at higher frequencies, possibly due to machine resonance or other artefacts. More accurate high frequency data may be obtained by measuring the shear stress–strain relation instead of the axial stress–strain relation. Future efforts will include a more in-depth investigation of the relationship between the ablation conditions and the viscoelastic properties of the tissue.

Acknowledgements

The authors wish to thank Larry Whitesell and Jennifer Buck from the Department of Cardiovascular Research for the tissue specimens. This study was funded in part by NIH grant 2 T32 CA-09206, and by the Whitaker Foundation grant RG-02–0457. The authors also thank Dr Udomchai Techavipoo for his assistance in sample preparation. Finally, a word of thanks goes to Dr Lawrence Taylor of the University of Rochester for his suggestions and comments.

References

Arbogast KB, Margulies SS. Material characterization of the brainstem from oscillatory shear tests. J Biomech 1998;31:801–7. [PubMed: 9802780]

Bagley RL, Torvik PJ. A theoretical basis for the application of fractional calculus to viscoelasticity. J Rheology 1983;27:201–10.

Chen EJ, Novakofski J, Jenkins WK, O'Brien WD Jr. Young's modulus measurements of soft tissues with application to elasticity imaging. IEEE Trans Ultrason Ferroelectr Freq Control 1996;43:191–4.

Chen, Q.; Suki, B.; An, KN. Dynamical mechanical properties of agarose gel by a fractional derivative model 2003. In: Soslowsky, LJ., editor. Summer Bioengineering Conference (Key Biscayne, FL). 2003.

Darvish KK, Crandall JR. Nonlinear viscoelastic effects in oscillatory shear deformation of brain tissue. Med Eng Phys 2001;23:633–45. [PubMed: 11755808]

Dickinson RJ, Hill CR. Measurement of soft tissue motion using correlation between A-scans. Ultrasound Med Biol 1982;8:263–71. [PubMed: 7101574]

Erkamp RQ, Wiggins P, Skovorada AR, Emelianov SY. Measuring the elastic modulus of small tissue samples. Ultrason Imaging 1998;20:17–28. [PubMed: 9664648]

Fung, YC. Biomechanics. New York: Springer; 1993.

Hall TJ, Bilgen M, Insana M, Krouskop T. Phantom materials for elastography. IEEE Trans Ultrason Ferroelectr Freq Control 1997;44:1355–65.

Han L, Noble JA, Burcher M. A novel ultrasound indentation system for measuring biomechanical properties of *in vivo* soft tissue. Ultrasound Med Biol 2003;29:813–23. [PubMed: 12837497]

Ishihara M, Sato M, Sato S, Kikuchi T, Fujikawa K, Kikuchi M. Viscoelastic characterization of biological tissue by photoacoustic measurement. Japan J Appl Phys 2003;42:L556–L8.

Kallel F, Bertrand M, Ophir J. Fundamental limitations on the contrast-transfer efficiency in elastography: an analytic study. Ultrasound Med Biol 1996;22:463–70. [PubMed: 8795173]

Kim SM, McCulloch TM, Rim K. Comparison of viscoelastic properties of the pharyngeal tissue: human and canine. Dysphagia 1999;14:8–16. [PubMed: 9828269]

Krouskop TA, Wheeler TM, Kallel F, Hall T. The elastic moduli of breast and prostate tissues under compression. Ultrason Imaging 1998;20:260–74. [PubMed: 10197347]

Lakes RS, Vanderby R. Interrelation of creep and relaxation: a modeling approach for ligaments. J Biomech Eng 1999;121:612–5. [PubMed: 10633261]

Lippert, S.; Grimm, MJ. Estimating the material properties of brain tissue at impact frequencies: a curve-fitting solution 2003. In: Soslowsky, LJ., editor. Summer Bioengineering Conference (Key Biscayne, FL). 2003.

Liu Z, Bilston L. On the viscoelastic character of living tissue: experiments and modeling of the linear behaviour. Biorheology 2000;37:191–201. [PubMed: 11026939]

Moffit TP, Baker DA, Kirkpatrick SJ, Prahl SA. Mechanical properties of coagulated albumin and failure mechanisms of liver repaired with the use of an argon-beam coagulator with albumin. J Biomed Mater Res 2002;63:722–8. [PubMed: 12418016]

Moskowitz, AJ.; Richards, MS.; Taylor, LS.; Lerner, AL. Modeling the visco-elastic response of bovine liver tissue 2001. In: Rajapakse, YDS., editor. ASME Int Mechanical Engineering Congress and Exposition (New York, NY). 2001.

Nasseri S, Bilston LE. Viscoelastic properties of pig kidney in shear, experimental results and modeling. Rheologica Acta 2002;41:180–92.

Ophir J, Cespedes I, Ponnekanti H, Yazdi Y, Li X. Elastography: a quantitative method for imaging the elasticity of biological tissues. Ultrason Imaging 1991;13:111–34. [PubMed: 1858217]

Sammani A, Bishop J, Luginbuhl C, Plewes DB. Measuring the elastic modulus of *ex vivo* small tissue samples. Phys Med Biol 2003;48:2183–98. [PubMed: 12894978]

Schwartz, J-M.; Langelier, È.; Moisan, C.; Laurendeau, D. Non-linear soft tissue deformations for the simulation of percutaneous surgeries. In: Neissen, W.; Viergever, M., editors. 4th Int Conf on Medical Image Computing and Computer-Assisted Intervention (Utrecht). 2001.

Suki B, Barabási A-L, Lutchen KR. Lung tissue viscoelasticity: a mathematical framework and its molecular basis. J Appl Physiol 1994;76:2749–59. [PubMed: 7928910]

Szabo TL, Wu J. A model of longitudinal and shear wave propagation in viscoelastic media. J Acoust Soc Am 2000;107:2437–46. [PubMed: 10830366]

Taylor, LS.; Lerner, AL.; Rubens, DJ.; Parker, KJ. A Kelvin–Voigt fractional derivative model for viscoelastic characterization of liver tissue 2002. In: Scott, EP., editor. ASME Int Mechanical Engineering Congress and Exposition (New Orleans, LA). 2002.

Taylor, LS.; Richards, MS.; Moskowitz, AJ.; Lerner, AL.; Rubens, DJ.; Parker, KJ. 2001 IEEE Ultrasonics Symposium. 2001. Viscoelastic effects in sonoelastography: impact on tumor detectability; p. 1639-42.

Taylor, LS.; Rubens, DJ.; Mejia, L.; Parker, KJ. ASME Int Mechanical Engineering Congress and Exposition (Washington, DC). 2003. Preliminary results of cyclic uniaxial compression of bovine liver 2003.

Wilson LS, Robinson DE. Ultrasonic measurement of small displacements and deformations of tissue. Ultrason Imaging 1982;4:71–82. [PubMed: 7199773]

Yeh WC, Li PC, Jeng YM, Hsu HC, Kuo PL, Li ML, Yang PM, Lee PH. Elastic modulus measurements of human liver and correlation with pathology. Ultrasound Med Biol 2002;28:467–74. [PubMed: 12049960]

Yuan H, Kononov S, Cavalcante FSA, Lutchen KR, Ingenito EP, Suki B. Effects of collagenase and elastase on the mechanical properties of lung tissue strips. J Appl Physiol 2000;89:3–14. [PubMed: 10904029]

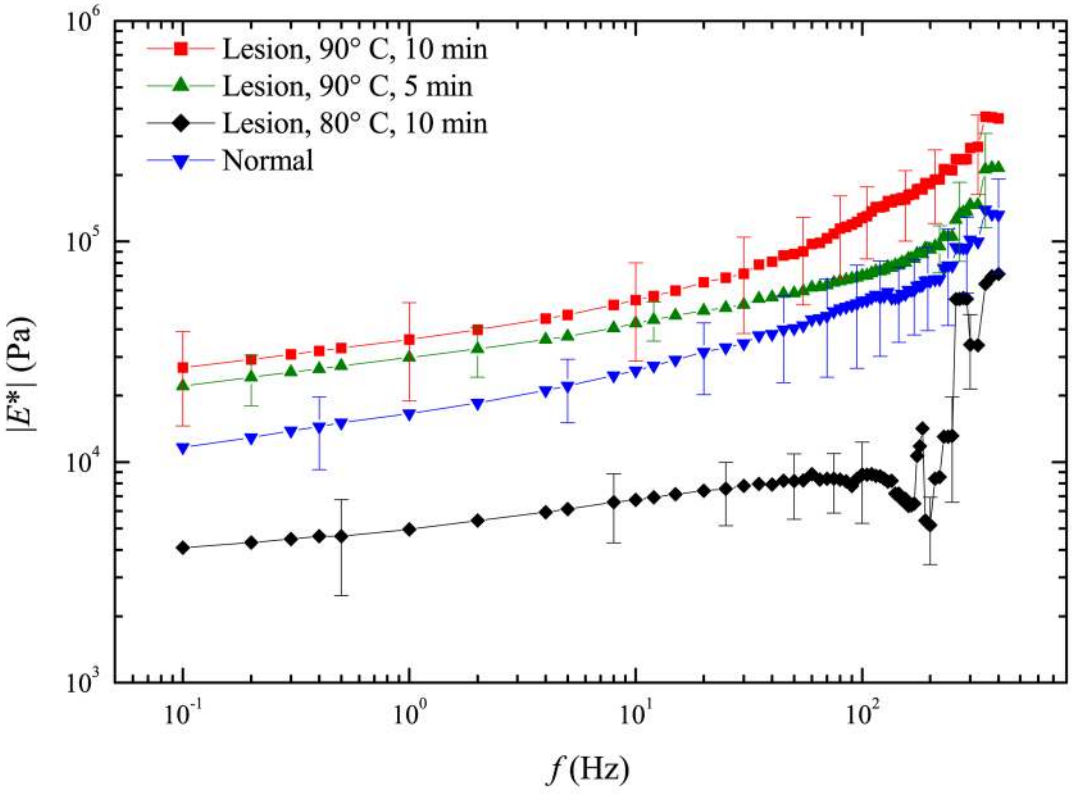

Figure 1.
Plot of the magnitude of the complex modulus as a function of stimulating frequency for canine liver tissue. Plots are shown for three thermal lesions prepared by rf ablation and for normal tissue.

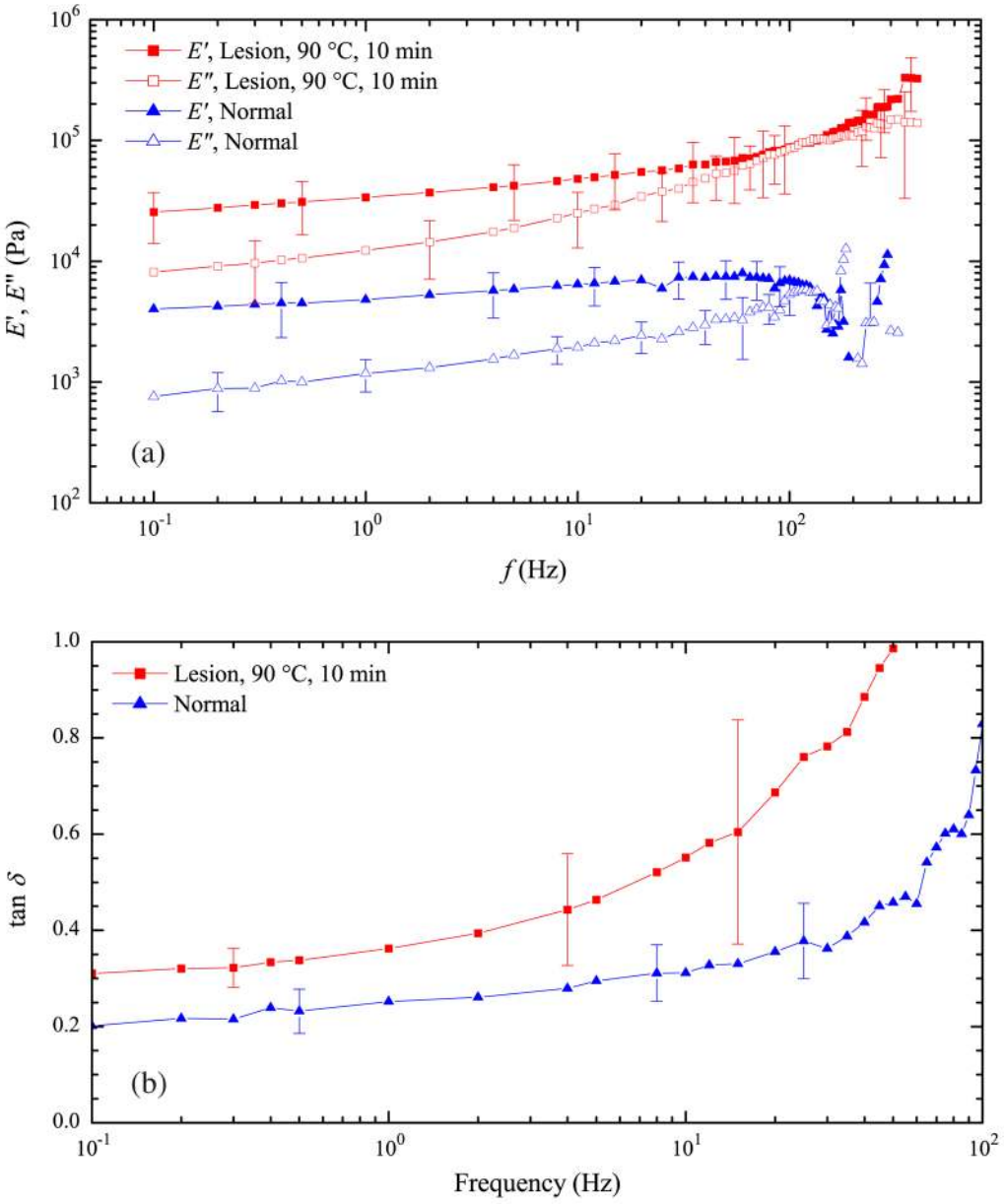

Figure 2.

(a) Plot of the real and imaginary parts of the complex modulus as a function of stimulating frequency for normal canine liver and a thermal lesion prepared at 90 °C for 10 min (b) Plot of the phase as a function of stimulating frequency for normal canine liver and the thermal lesion prepared at 90 °C for 10 min. Due to the presence of experimental artefacts at high frequencies, the plot is truncated to 100 Hz.

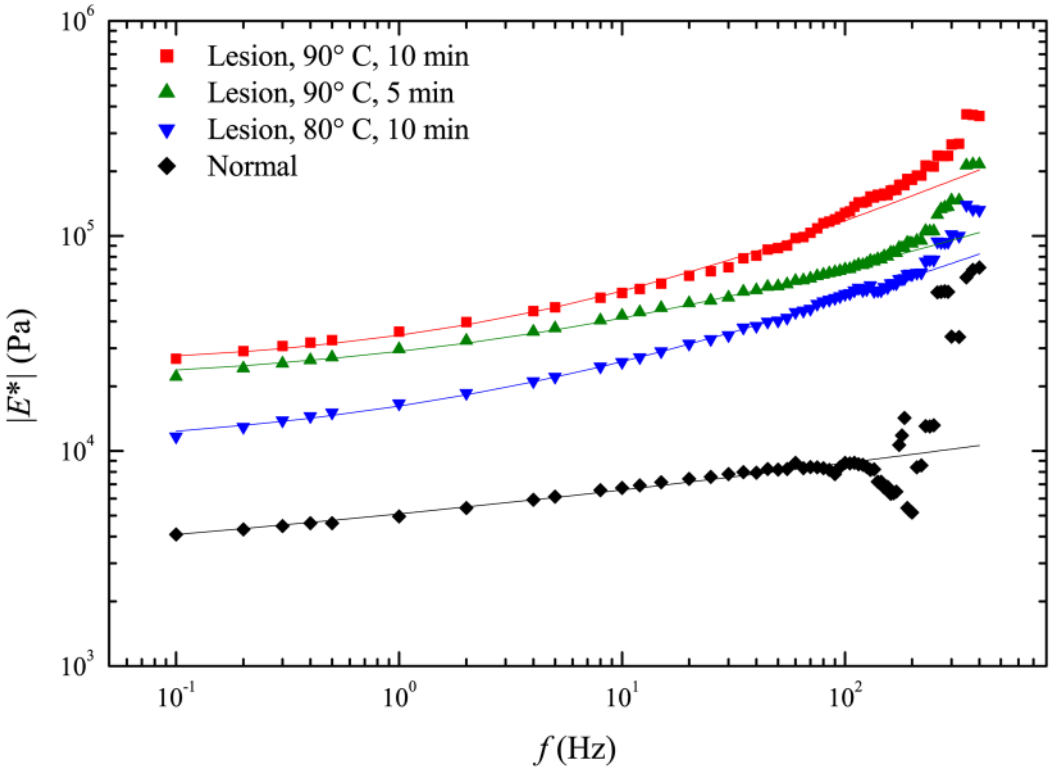

Figure 3.
Plot of the magnitude of the complex modulus of the KVFD model as a function of stimulating frequency with nonlinear least squares fitting results overlaid.

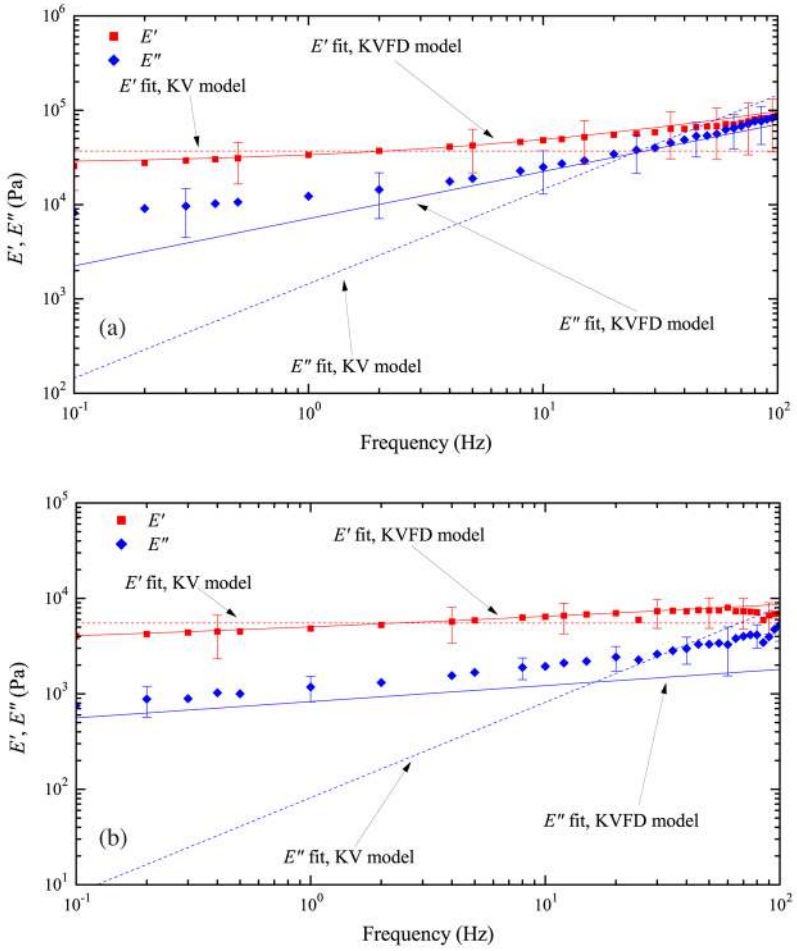

Figure 4.

Plot of the real and imaginary parts of the complex modulus as a function of frequency for (a) a thermal lesion prepared at 90 °C for 10 min and (b) normal tissue. Results from the least squares fit for both the KVFD and KV models have been overlaid.

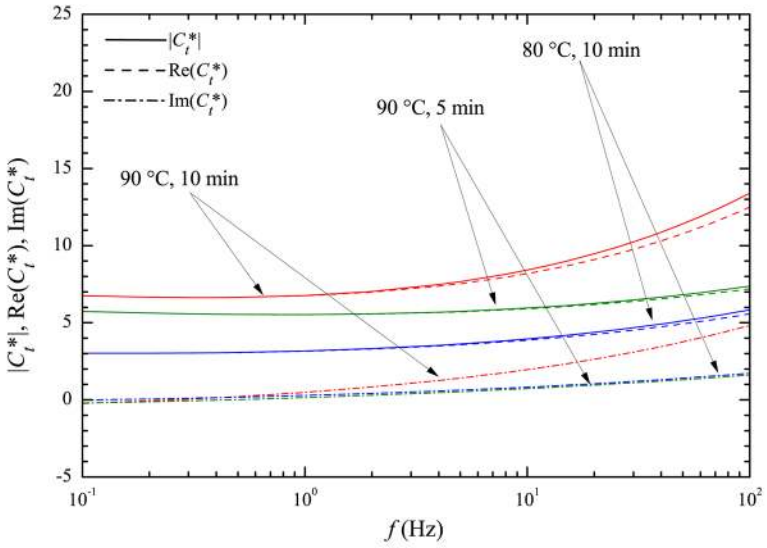

Figure 5.
Plot of the complex modulus contrast as a function of stimulating frequency.

Table 1

Best-fit parameters for canine liver tissue using the KVFD model.

Tissue	No. of specimens	E_0 (Pa)	η (Pa s$^{\alpha}$)	α	χ^2	R^2
Normal	10	1 995 ± 40	2 310 ± 54	0.169 ± 0.005	0.001 13	0.9832
Lesion, 90 °C, 10 min	10	26 600 ± 780	4 000 ± 390	0.500 ± 0.016	0.001 36	0.9940
Lesion, 90 °C, 5 min	5	16 300 ± 500	8 000 ± 390	0.297 ± 0.007	0.000 13	0.9991
Lesion, 80 °C, 10 min	5	10 000 ± 320	3 300 ± 210	0.400 ± 0.01	0.000 51	0.9979

Table 2

Best-fit parameters for canine liver tissue using the KV model ($\alpha = 1$).

Tissue	No. of specimens	E_0 (Pa)	η (Pa s)	α	χ^2	R^2
Normal	10	5 500 ± 250	13.0 ± 1.3	1.0	0.032 58	0.532 9
Lesion, 90 °C, 10 min	10	37 000 ± 2000	230 ± 13	1.0	0.036 26	0.834 6
Lesion, 90 °C, 5 min	5	31 000 ± 1700	125 ± 9	1.0	0.040 9	0.709 51
Lesion, 80 °C, 10 min	5	17 000 ± 1100	101 ± 7	1.0	0.050 9	0.775 6